Available online www.jocpr.com

Journal of Chemical and Pharmaceutical Research, 2014, 6(10):18-26

Research Article

ISSN : 0975-7384
CODEN(USA) : JCPRC5

DFT study of half-sandwich bis (tetramethylaluminate) lanthanide complexes

Houria Bennaceur and Nadia Ouddai

Laboratoire de chimie des matériaux et des vivants: Activité, Réactivité, University, Hadj Lakhdar, Batna, Algeria

---

ABSTRACT

Electronic structure of the half-sandwich complexes [Ln(AlMe$_4$)$_2$Cp^R] with (Ln=Lu, Y, La), (Cp^R = 1,3-(Me$_3$Si)$_2$C$_5$H$_3$ and C$_5$Me$_5$), has been investigated using density functional theory method at the ZORA/PW91/TZP level. The study reveals that the twist angle θ decreases with increasing ionic radii and the effect of substitution,1, 3-(Me$_3$Si)$_2$C$_5$H$_3$ on the occupied molecular orbitals, ensuring a great stability. The quantum theory of atoms in molecules (AIM) and energy decomposition analysis indicate that the substitution 1, 3-(Me$_3$Si)$_2$C$_5$H$_3$ increases the degree of covalency in the bonding Cp^{R}Ln (Lu^{+3}, Y^{+3}, La^{+3})–(AlMe$_4$)$_2$. According to the Pearson terminology, The La(AlMe$_4$)$_2$(1,3-(Me$_3$Si)$_2$C$_5$H$_3$) complex shows the higher acidity.

Keywords: lanthanides, Cyclopentadienyl ligands, DFT, Half-Sandwich, Acidity Strength, AIM, Dipole moment

---

INTRODUCTION

Lanthanide complexes have very rich and diversified coordinating properties and reactivities, and have been vastly used in organic and polymer synthesis [1]. Monocyclopentadienyl or half-sandwich complexes have recently attracted considerable attention in organorare-earth metal chemistry [2-4]. The rare earth metals usually adopt the +3 oxidation state as the most stable oxidation state [5]. Recently, the complexes half-sandwich bis(tetramethylaluminate) lanthanide complexes of the type Ln(AlMe$_4$)$_2$Cp^R containing various substituted cyclopentadienyl ancillary ligands have been synthesized and characterized by X-ray structure analysis [6-8]. These complexes are active in isoprene polymerization as precatalyst with boron-containing cocatalysts, such as [Ph$_3$C] [B (C$_6$F$_5$)$_4$], [PhNMe$_2$H][B-(C$_6$F$_5$)$_4$], or B(C$_6$F$_5$)$_3$ produces initiators for the fabrication of trans -1, 4-polyisoprene [6]. Within this framework, we found interesting to consider a series of half-sandwich complexes [Ln(AlMe$_4$)$_2$Cp^R), Ln=(Lu, Y, La) and Cp^R=(1,3-(Me$_3$Si)$_2$C$_5$H$_3$, C$_5$Me$_5$)] (see scheme 1) to understand some peculiar geometries, proprieties and chemical reactivity. The aim of our work is also to investigate further the nature of bonding between metal and ligand. In our study we will make use of density functional theory (DFT) calculations. DFT is an effective tool for the determination of structural arrangements of organometallic molecules [9].

EXPERIMENTAL SECTION

Computational Method

Our calculations were performed using the Amsterdam density functional (ADF) program developed by Baerends and co-workers [10]. Electron correlation was treated within general gradient approximation with the PW91 functional [11]. The atom electronic configurations were described by a triple ζ Slater type orbital (STO) basis set for H 1s, and 2s and 2p for C, 3s and 3p for Al, and Si, augmented with 2p single-ζ polarization functions for H atoms, with 3d single-ζ polarization functions for C and 4p single-ζ polarization functions for Al and Si. The atomic basis set of the lanthanide atoms is the following: a triple ζ -STO for the outer 4f, 5d, and 6s orbitals, a frozen core

approximation for the shells of lower energy. Relativistic corrections were taken into account with the use of the relativistic scalar zero-order-regular approximation method [12]. The bonding interactions have been analyzed by means of Morokuma-type energy decomposition analysis (decomposition of the bonding energy into the Pauli (exchange) repulsion, total steric interaction, and orbital interaction terms) [13], developed by Ziegler and Rauk for DFT methods and incorporated in ADF [14]. The basis set superposition error was assessed on complexes. The topological analyses were calculated with Dgrid [15], using tape 21 file exported from ADF.

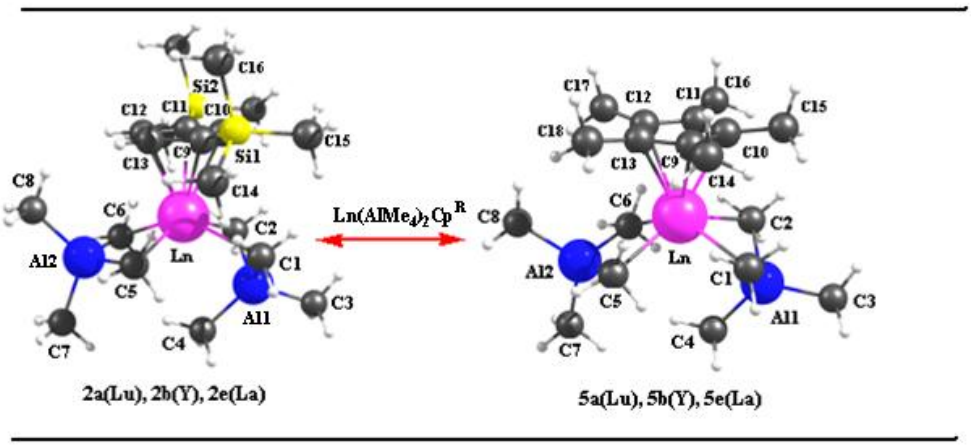

Scheme 1

RESULTS AND DISCUSSION

Molecular geometry optimization

The optimized geometrical parameters and the available experimental data are summarized in Table 1 for the molecular structures 2a, 2b, 2e, 5a, 5b and 5e. They are given relevant optimized bond distances and angles values for the Y, La, Lu complexes are closed shell systems, their fundamental state are singlet state computed at the ZORA/PW91 /TZP level. The geometries were fully optimized in Cs for 2a, 2b, 2e and no symmetry for 5a, 5b, 5e without constraints. First of all, it can be seen in Table 1, there is good overall agreement between optimized and X-ray data. Nevertheless, the distances Ln-C_1, Ln-C_2, Ln-C_5 and Ln-C_6 (2.647 Å, 2.725 Å, 2.644 Å, 2.904 Å, 2.892 Å, 2.529 Å, 2.589 Å, 2.547 Å, 2.763 Å, 2.548 Å, 2.757 Å) are respectively somewhat higher of 0.084 Å, 0.101 Å, 0.072 Å, a maximum deviation 0.102 Å, 0.098 Å, 0.012 Å, 0.029 Å, 0.046 Å, 0.056 Å, 0.047 Å and 0.063 Å as obtained by X-ray diffraction. This overestimation may have resulted as a consequence of the selected theoretical method and molecular systems chosen in our present investigation. The distances calculated Ln-Cp and Ln-Cg(ring centroid), Ln-Al, Ln-C (Table1) increase with increase of the ionic radii of the lanthanide ions in the series [16], La > Y > Lu.

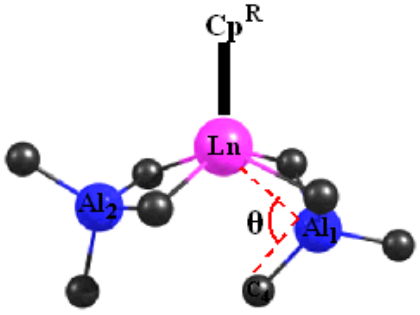

Scheme 2

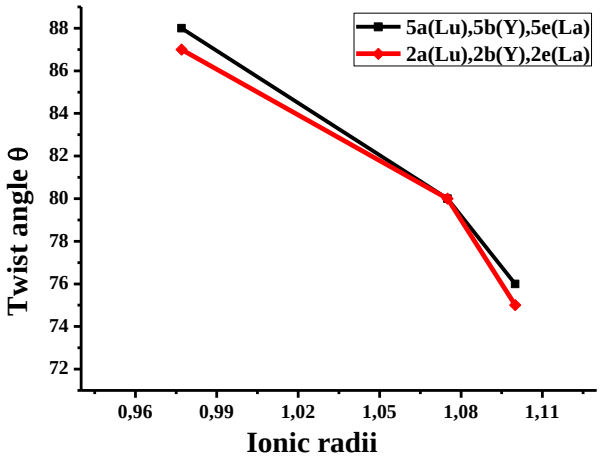

Fig. 1 Evolution of Twist angle θ for $Ln(AlMe_4)_2Cp^R$

The twist angle θ for $Ln(AlMe_4)_2Cp^R$ (Scheme 2, Table 2, Fig 1) varies from 75° to 88° and decreases with increasing ionic radii 2e < 2b < 2a and 5e < 5b < 5a. But the trend for twist angle θ in both complexes 2b, 5b are similar. For 2a, 5a and 2e, 5e there are clearly two different behaviors.

Table 1. Computed and experimental structural data in gras of $Ln(AlMe_4)_2Cp^R$ complexes

	Bond length (A°)								
	Ln-(Cp)	**Ln-Cg**	**Ln-C_1**	**Ln-C_2**	**Ln-C_5**	**Ln-C_6**	**Ln…C_4**	**Ln-Al_1**	**Ln-Al_2**
2a(Lu)	2.627-2.648	2.34	2.647	2.647	2.529	2.529	3.461	2.941	3.047
	2.580(2)–2.596(1)	**2.29**	**2.563(1)**	**2.563(1)**	**2.517(1)**	**2.517(1)**	**3.492(2)**	**2.913(5)**	**3.029(5)**
2b(Y)	2.681-2.697	2.39	2.725	2.725	2.589	2.589	3.271	2.949	3.103
	2.620(3)–2.641(2)	**2.34**	**2.624(2)**	**2.624(2)**	**2.560(2)**	**2.560(2)**	**3.302(3)**	**2.913(9)**	**3.078(1)**
2e(La)	2.849-2.859	2.58	2.909	2.909	2.732	2.732	3.214	3.069	3.276
5a(Lu)	2.633-2.636	2.33	2.644	2.644	2.547	2.548	3.503	2.943	3.094
	2.566(3)-2.603(3)	**2.28**	**2.572(3)**	**2.597(3)**	**2.501(3)**	**2.501(3)**	**3.447**	**2.913(9)**	**3.061(9)**
5b(Y)	2.684-2.689	2.39	2.731	2.722	2.610	2.608	3.260	2.939	3.152
5e(La)	2.831-2.845	2.56	2.904	2.892	2.763	2.757	3.247	3.075	3.319
	2.753(2)-2.801(3)		**2.802(4)**	**2.794(3)**	**2.707(3)**	**2.694(3)**	**3.140(3)**	**3.014(9)**	**3.268(9)**
	Bond angle length (°)								
	Al_1-Ln-Al_2	**C_1-Ln-C_2**	**C_5-Ln-C_6**		**C_1-Al1-C_2**		**C_5-Al_2-C_6**	**Al_1-Ln-Al_2**	
2a(Lu)	114	77	85		105		108	114	
	114(1)	**79(5)**	**84(5)**		**105(7)**		**108(6)**	**114(1)**	
2b(Y)	117	76	84		107		19	117	
	117(3)	**78(1)**	**83(1)**		**106(1)**		**109(1)**	**117(3)**	
2e(La)	118	70	79		108		111	118	
5a(Lu)	113	79	84		108		108	113	
	112(2)	**80(1)**	**84(1)**		**107(1)**		**108**	**112(2)**	
5b(Y)	115	77	82		109		110	115	
5e(La)	117	72	78		110		111	117	
	117	**73(1)**	**78(1)**					**117**	

Table 2. Twist angle θ (°) for $Ln(AlMe_4)_2Cp^R$

	2a(Lu)	**2b(Y)**	**2e(La)**	**5a(Lu)**	**5b(Y)**	**5e(La)**
θ (°)	87	80	75	88	80	76

Frontier Molecular Orbital Properties:

The frontier molecular orbital compositions and energy levels of 2a, 2b, 2e, 5a, 5b and 5e are shown in Table 3, Fig.2 and Scheme 3, respectively. A large gap vary from 3.26 to 3.80 eV, separates the lowest unoccupied molecular orbital LUMO from the highest occupied molecular orbital HOMO, ensuring the good stability of 2a, 2b, 2e, 5a, 5b and 5e (see Fig. 2). As shown in Fig. 2, the stabilization of the HOMO level is more prominent in 2a than that of all compounds, and the order of stabilization of the HOMO energy levels is as follows: 2a (-5.69 eV) > 2b (-5.63eV) > 2e (-5.56 eV) > 5a (-5.34 eV) > 5b (-5.31eV) > 5e (-5.14eV), which is consistent with the nature of metal and the

ligand. The HOMO of 2a, 2b and 2e is essentially a σ bonding orbital, is mainly composed of Al Px (4.0%d*yz* + 18.0%P*x*) and methyl group (78.0%). As shown in Fig. 2, the silyl ligand do not play a significant role on the composition of HOMO for 2a, 2b and 2e, but with respect to 5a, 5b and 5e, It is obvious in Fig. 2 that in the HOMO the Ln d orbital (10%) is bonding with the Cp (90%) group. The effect of substituent 1,3-$(Me_3Si)_2C_5H_3$ on the highest occupied molecular orbital's, particularly the difference in energy and composition of HOMO's compounds 2 and 5. Indeed, the substitution of carbon by silicon in compound 5 generates compounds 2. The binding nature and composition of the HOMO's compounds 5 explains the rearrangement of high occupied molecular orbital's in 2.

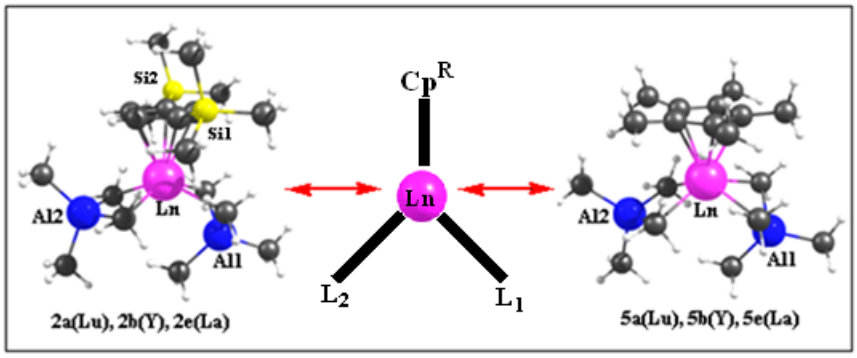

Scheme 3

Table 3. Energies (ε.eV) and percentage compositions of selected orbitals (MO) in the Homo-Lumo region of complexes $Ln(AlMe_4)_2Cp^R$

OM	Energy(eV)	Occu	Ln%	Cp^R%(Si%)	L_1%(Al%)	L_2%(Al%)
2a(Lu)						
Homo-2	-5.98	2	0	1(0)	99(21)	0
Homo-1	-5.83	2	6	86(2)	5(0)	3(0)
Homo	-5.69	2	0	0	0	100(22)
Lumo	-1.88	0	66	34(0)	0	0
2b(Y)						
Homo-2	-6.00	2	3	70(0)	10(3)	17(4)
Homo-1	-5.83	2	6	86(2)	5(0)	3(0)
Homo	-5.63	2	0	0	0	100(22)
Lumo	-2.15	0	80	20(0)	0	0
2e(La)						
Homo-2	-5.81	2	5	7(0)	23(2)	65(7)
Homo-1	-5.73	2	7	87(2)	3(0)	3(0)
Homo	-5.56	2	0	0	0	100(22)
Lumo	-2.18	0	82	18(0)	0	0
OM	**Energy(eV)**	**Occup**	**Ln%**	**Cp^R%**	**L_1%(Al%)**	**L_2%(Al%)**
5a(Lu)						
Homo-2	-5.57	2	0	0	0	100(22)
Homo-1	-5.37	2	10	90	0	0
Homo	-5.34	2	10	90	0	0
Lumo	-1.61	0	66	26	4(0)	4(0)
5b(Y)						
Homo-2	-5.47	2	0	0	0	100(22)
Homo-1	-5.36	2	9	91	0	0
Homo	-5.31	2	11	89	0	0
Lumo	-1.90	0	75	19	4(0)	2(0)
5e(La)						
Homo-2	-5.45	2	0	0	0	100(21)
Homo-1	-5.22	2	11	89	0	0
Homo	-5.14	2	10	90	0	0
Lumo	-1.88	0	86	14	0	0

The composition of the LUMO of 2a, 2b, 2e, 5a, 5b and 5e is a π and π* orbital localized on the lanthanide atom and cyclopentadienyl ligand, with more than 60% composition metallic, showing that the tetramethylaluminate ligands do not cause a significant change in LUMO distribution. The orbital energy levels of HOMO and LUMO are influenced by changing the lanthanide and the substituent in cyclopentadienyl ligand. The LUMO energy level of

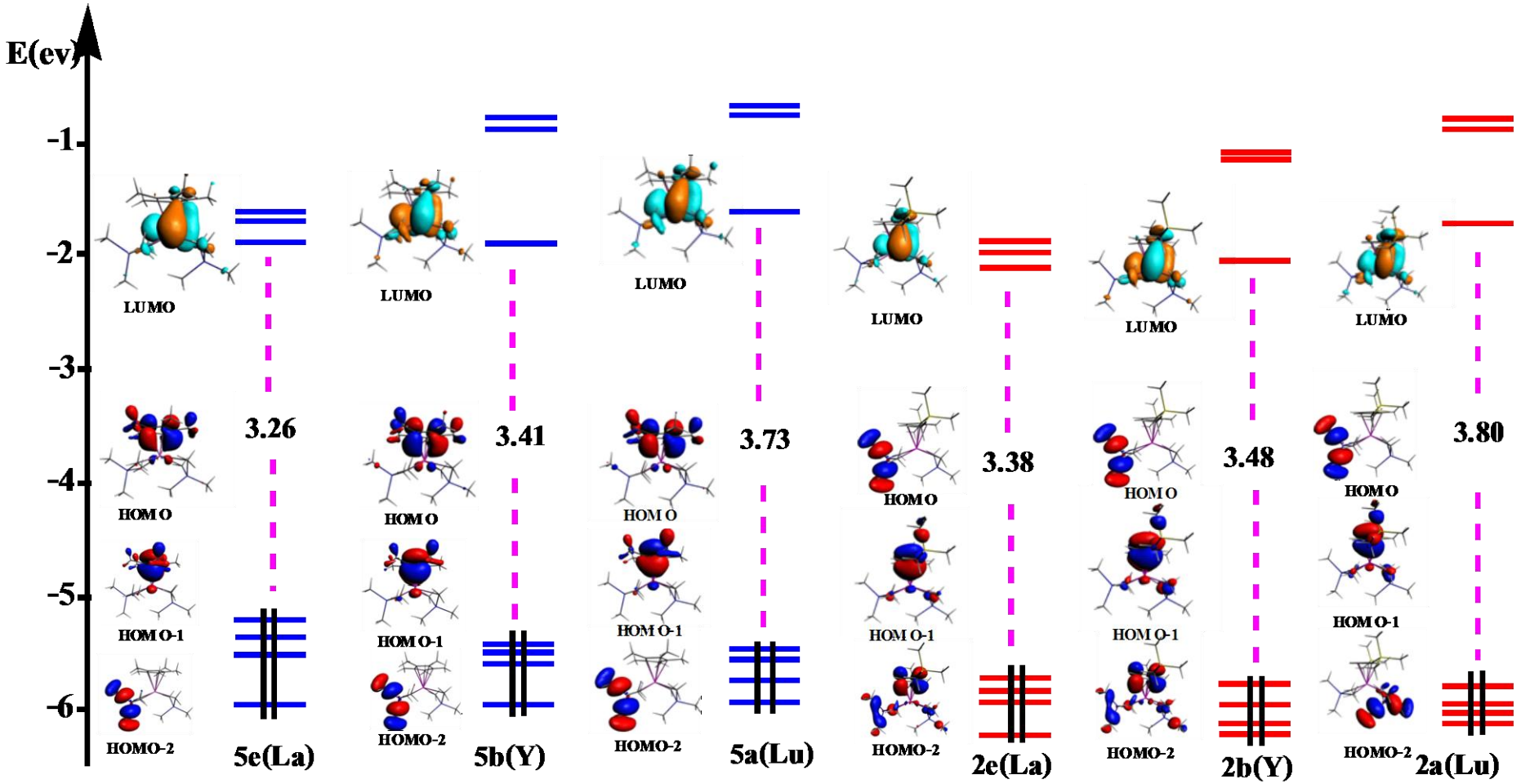

Fig. 2 Comparative MO diagrams of the studied systems

5e, 5b and 2a are comparable with only 0.02 eV stabilization for 5b, which results in the broader HOMO-LUMO gap in 2a (3.80 eV) than in 5e (3.26 eV). This indicates that the effect of the energy of the π* orbital is negligible.

Population Analysis and Dipole Moments

Table 4 shows the atomic net charges for 2a, 2b, 2e, 5a, 5b and 5e complexes, obtained using the Hirshfeld analysis [17]. In all neutral complexes, the carbon atoms are negatively charged. Interestingly, only the net negative charge on the carbons of the cyclopentadienyl is high in the case of the 2a, 2b and 2e, this suggests that the electronic donation of $SiMe_3$ is limited to Cp. The different metal and carbon charges in the half-sandwich species establish polarized structures (Table 4), an observation that is confirmed by the computed dipole moments, which are also good descriptors of the ground-state total charge distribution. Larger dipole moments are calculated for the half-sandwich species, amounting to 3.60 and 4.50 D for 2a and 5b, respectively, due the particular orientation of the $SiMe_3$ group tethered to 2a, 2b, 2e for the former and the negative C_5Me_5 at 5a, 5b, 5e for the latter.

Table 4. Hirshfeld charge analysis and Dipole Moments

	2a(Lu)	2b(Y)	2e(La)	5a(Lu)	5b(Y)	5e(La)
Ln	0.678	0.652	0.683	0.667	0.639	0.672
Al_1	0.357	0.361	0.362	0.357	0.360	0.362
Al_2	0.366	0.366	0.364	0.365	0.365	0.363
C_1	-0.241	-0.241	-0.240	-0.238	-0.238	-0.239
C_2	-0.241	-0.241	-0.240	-0.238	-0.238	-0.239
C_3	-0.264	-0.263	-0.265	-0.265	-0.264	-0.267
C_4	-0.256	-0.250	-0.243	-0.258	-0.250	-0.244
C_5	-0.239	-0.240	-0.236	-0.238	-0.240	-0.237
C_6	-0.239	-0.240	-0.236	-0.238	-0.240	-0.237
C_7	-0.267	-0.267	-0.269	-0.269	-0.268	-0.270
C_8	-0.270	-0.270	-0.269	-0.268	-0.268	-0.269
C_9	-0.124	-0.121	-0.127	-0.036	-0.033	-0.037
C_{10}	-0.074	-0.071	-0.075	-0.032	-0.030	-0.035
C_{11}	-0.124	-0.121	-0.127	-0.035	-0.032	-0.038
C_{12}	-0.072	-0.070	-0.073	-0.036	-0.033	-0.036
C_{13}	-0.072	-0.070	-0.073	-0.036	-0.032	-0.035
C_{14}	-0.201	-0.201	-0.201	-0.105	-0.104	-0.105
Cp	-0.319	0.304	-0.329	-0.176	-0.162	-0.183
Si	0.378	0.380	0.378	-	-	-
μ (debye)	3.602	3.603	3.658	4.292	4.509	4.439

Energy-decomposition analysis

The $Cp^RLn–(AlMe_4)_2$ bond dissociation energy was computed for 2a, 2b, 2e, 5a, 5b and 5e, considering a heterolytic process, i.e., the bonding energy (BDE) between $[Cp^RLn]$ (Ln = Lu, La and Y) and $(AlMe_4)_2$ fragments. The advantage of this approach is to estimate the interaction energy BDE between the metal center and the tetramethylaluminate group, as the sum of the energy contributions of the stabilizing orbital interaction Eorb, and repulsion interactions Epauli:

$$BDE=Eelec+Eorb+Epauli$$

Eelec is the classical electrostatic interaction between the charge distributions of the interacting fragments in their unrelaxed geometry. Epauli roughly corresponds to the energy issued of the interaction between the occupied orbitals of the fragments. Eorb mainly accounts for the interaction between occupied and vacant orbitals. The latter can be decomposed into σ and π components, which were calculated using the procedure implemented in the ADF code [14,13].

Table 5. Various energy contributions

	E_{elec}	$E_{orb}+E_{pauli}$	BDE
2a(lu)	-18.16	-3.00	-21.17
2b(Y)	-17.01	-3.34	-20.35
2e(La)	-16.46	-2.84	-19.30
5a(Lu)	-18.05	-2.76	-20.72
5b(Y)	-16.97	-2.88	-19.85
5e(La)	-16.49	-2.30	-18.79

Comparison of the BDE values (Table 5) computed for the six complexes indicates that the $Cp^RLn–(AlMe_4)_2$ bonding presents a weak ionic character and is slightly stronger in 2a than in other molecules. The substitution 1, 3-$(Me_3Si)_2C_5H_3$ increases the covalency degree in the $Cp^RLn–(AlMe_4)_2$ bonding (see Table 6).

Table 6. Percentage of electrostatic and orbital contributions to the $Cp^RLn–(AlMe_4)_2$ bonding

	2a(Lu)	2b(Y)	2e(La)	5a(Lu)	5b(Y)	5e(La)
%Eorb	14	16	15	13	15	12
%Eele	86	84	85	87	85	88

The topological analysis of AIM

The half-sandwich complexes $Ln(AlMe_4)_2Cp^R$ contain two ligands, Cp^R and $AlMe_4$. The ligand Cp^R displayed η5 coordination [18], to the metal center in these complexes. The coordinational flexibility of the $[AlMe_4]$ ligand, as evidenced by $\eta^{1/2/3}$ coordination modes [8]. This coordination has been analyzed by AIM approach of Bader and coworkers [19, 20]. This method tells us that there is one bond critical point (BCP) between each pair of atoms that are bonded to one another and describes chemical bonding in terms of bond critical points (BCPs) and bond paths. The values of the electronic charge density, ρ(r), Laplacian , $\nabla^2\rho(r)$, and the energy density, H(r), at the Lanthanide-Carbon BCPs of the complexes under study (see Table 7, Fig. 3).

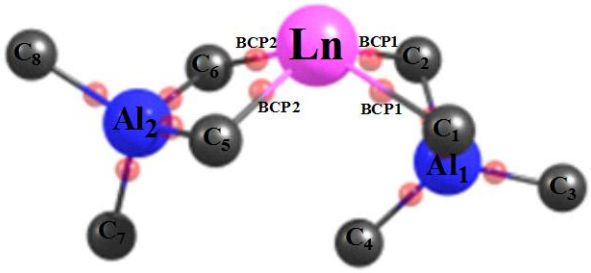

Fig. 3 Molecule Graph of $Ln(AlMe_4)_2$, BCPs (red)

In general, ρ(r) is greater than 0.20 a.u., $\nabla^2\rho(r) < 0$ in covalent bonding and ρ(r) less than 0.10 a.u., $\nabla^2\rho(r) > 0$ in a closed-shell interaction (e.g., ionic, van der Waals, or hydrogen) [20]. The low value of the electronic density at the Lanthanide – ligand critical point (ρ(r) ≈ 0.03 a.u.) and the strong local depletion (Laplacian> 0) confirm an electrostatic interaction between the Lanthanide and the Carbon atoms of the ligands. The covalent partial character of the bond in all complexes indicated by the small negative values (-0.0007 to -0.0051 in Table 7) for the term H(r) at the BCP of the Ln-C bond path [9].

Table 7. Topological properties at Ln-C BCP's of $Ln(AlMe_4)_2$

	Critical Points	ρ(r)	$\nabla^2\rho(r)$	H(r)
2a(Lu)	BCP1	0.0356	0.0922	-0.0034
	BCP2	0.0417	0.1130	-0.0051
2b(Y)	BCP1	0.0300	0.0828	-0.0007
	BCP2	0.0360	0.1031	-0.0019
2e(La)	BCP1	0.0281	0.0685	-0.0010
	BCP2	0.0345	0.0932	-0.0020
5a(Lu)	BCP1	0.0359	0.0924	-0.0036
	BCP2	0.0394	0.1112	-0.0043
5b(Y)	BCP1	0.0299	0.0820	-0.0007
	BCP2	0.0337	0.1011	-0.0012
5e(La)	BCP1	0.0280	0.0686	-0.0010
	BCP2	0.0321	0.0890	-0.0015

Acidity Strength

Chemical hardness is associated with the stability and reactivity of a chemical system. On the basis of frontier molecular orbital's, chemical hardness corresponds to the gap between the HOMO and LUMO. Chemical hardness was calculated as [21].

$$\eta = E_L - E_H$$

The low reactivity of a molecule is attributed to its wide energy gap HOMO-LUMO. Table 8 contains the computed chemical hardness values for the six compounds. The results indicate that 2a is the harder and less reactive than all complexes. Electronic chemical potential is defined as the negative of electronegativity of a molecule [22], and determined using equation.

$$\mu = (E_H + E_L)/2$$

Physically, μ describes the escaping tendency of electrons from an equilibrium system. The values of μ for the six complexes are presented in Table 8. The trend in electronic chemical potential is 5a (-3.47 eV) > 5e (-3.51eV) > 5b (-3.60 eV) > 2a (-3.78 eV) > 2e (-3.87 eV) > 2b (-3.89 eV). The largest electronic chemical potential is attributed to the most reactive complex. In conclusion the substitution decreases the reactivity. The global electrophilicity index, is a measure of the molecule's ability to accept electrons [23], was approximated by

$$\omega = (\mu^2 / 2\eta)$$

Electrophilicity index quantifies the energy stabilization in energy after a system accepts additional electronic charge from another species. The electrophilicity values for 2b and 2e complexes are the greater, which exhibit that these systems are the strong Lewis acids.

Table 8. Overall reactivity descriptors (ev)

	μ	η	ω	E_{LUMO}	E_{HOMO}
2a(Lu)	-3.78	3.80	1.88	-1.886	-5.690
2b(Y)	-3.89	3.48	2.17	-2.152	-5.631
2e(La)	-3.87	3.37	2.22	-2.186	-5.564
5a(Lu)	-3.47	3.73	1.61	-1.611	-5.342
5b(Y)	-3.60	3.41	1.90	-1.901	-5.314
5e(La)	-3.51	3.25	1.89	-1.889	-5.148

CONCLUSION

Electronic structure of half-sandwich $Ln(AlMe_4)_2Cp^R$ complexes have been investigated. Geometrical analysis suggest that the twist angle θ obtained for La $(AlMe_4)_2$(1, 3-$(Me_3Si)_2C_5H_3$) and La$(AlMe_4)_2(C_5Me_5)$ θ =75° and 76° respectively, can be correlated to the precatalytic reactivity. Based on this analysis, La$(AlMe_4)_2$(1, 3-$(Me_3Si)_2C_5H_3$) , La$(AlMe_4)_2(C_5Me_5)$ are the best precatalysts. AIM and energy decomposition analysises indicate a majority ionic bonding in all systems, the most significant is obtained with La $(AlMe_4)_2(C_5Me_5)$ (Eorb(88%),Eele(12%)), and that the substitution 1,3-$(Me_3Si)_2C_5H_3$ increases the degree of covalency bonding. The quantique analysis identified Y$(AlMe_4)_2$(1,3-$(Me_3Si)_2C_5H_3$) and La$(AlMe_4)_2$(1,3-$(Me_3Si)_2C_5H_3$) as two good precatalysts classified by their high acidity.

Acknowledgements

The authors are very thankful to the « Université Lyon 1 and CNRS UMR 5180 Sciences Analytiques; Laboratoire de Chimie Physique Théorique, bâtiment Dirac, 43 boulevard du 11 Novembre 1918, 69622 Villeurbanne Cedex (France) » for offering the computing facilities and helpful discussion with the scientists.

REFERENCES

[1] Peng Cui; Yaofeng Chen; Xin Xu and Jie Sun, *The Royal Society of Chemistry*., **2008**,11(43), 5547-5549.
[2] Andreas Fischbach; Eberhardt Herdtweck; Reiner Anwander, *Inorganica Chimica Acta*., **2006**, 359(15), 4855-4864.
[3] Erwan Le Roux; Yucang Liang; Karl W Törnroos; François Nief; Reiner Anwander, *Organometallics*, **2012**, 31(18), 6526-6537.
[4] Lars N Jende; Cäcilia Maichle Mössmer; Christoph Schädle; Reiner Anwander, *Journal of Organometallic Chemistry*., **2013**, 744(1), 74-81.
[5] Zhaomin Hou; Yunjie Luo; Xiaofang Li, *Journal of Organometallic Chemistry*., **2006**, 691(14), 3114-3121.
[6] Reiner Anwander; Michael G Klimpel; Martin Dietrich H; Dmitry J Shorokhovb and Wolfgang Scherer, *The Royal Society of Chemistry.*, **2003**, 48(73), 1008-1011.
[7] H Martin Dietrich; Clemens Zapilko; Eberhardt Herdtweck; Reiner Anwander, *Organometallics*., **2005**, 24(23), 5767-5771.
[8] Melanie Zimmermann; Karl W Tçrnroos; Helmut Sitzmann; and Reiner Anwander; *Chem. Eur. J.*, **2008**, 14(24), 7266-7277.
[9] Salima Lakehal; Nadia Ouddai; Douniazed Hannachi, Mohmed Bououdina, *Journal of Quantum Chemistry*., **2012**,9(1), 1-6.
[10] E J Baerends; D E Ellis; P Ros, *Chem Phys*., **1973**, 2(1), 41-51.
[11] J P Perdew; J A Chevary; S H Vosko; K A Jackson; M R Pederson; D J Singh; C Fiolhais, *Phys Rev B*., **1992**, 46(11), 6671-6687.
[12] E Van Lenthe; A. Ehlers; E J Baerends, *J Chem Phys*., **1999**, 110(18), 8943-8953.
[13] F M Bickelhaupt; E J Baerends; In: Rev Comput Chem, K B Lipkowitz; D B Boyd, Eds,Wiley-VCH: New York., **2000**, 15(1).1–86.
[14] T Ziegler; A Rauk; *Inorg, Chem*., **1979**, 18(6), 1558-1565.
[15] M Kohout, program DGrid, Version 4.3, **2008**.
[16] Salima Lakehal; Nadia Ouddai, *J. Rare Earths*., **2010**, 28(2), 161-165.
[17] F L Hirshfeld,*Theor, Chim. Acta*., **1977**, 44(2), 129-138.
[18] Dominique Robert; P Thomas; Spaniol; and Jun Okuda, *Eur J. Inorg Chem*., **2008**, 2008(18), 2801-2809.
[19] R F W Bader. Atoms in Molecules - A Quantum Theory, Oxford University Press: Oxford, **1990**.
[20] Matta C F, Boyd R J. The Quantum Theory of Atoms in Molecules: From Solid State to DNA and Drug Design, Eds. Wiley-VCH: Weinheim **2007**, 1-13.
[21] H Chermette, *J. Comput Chem*., **1999**, 20 (1), 129-154.
[22] Robert G Parr; Ralph G Pearson, *J. Am Chem Soc*., **1983**, 105(26): 7512-7516.
[23] Robert G Parr; László v Szentpály and Shubin Liu, *J. Am Chem Soc.*, **1999**, 121(9), 1922-1924.